REPORT DOCUMENTATION PAGE

Form Approved
OMB No. 0704-0188

1. AGENCY USE ONLY (Leave blank)	2. REPORT DATE	3. REPORT TYPE AND DATES COVERED
	1/14/96	Final Tech.Report 8/15/91-11/14/95

4. TITLE AND SUBTITLE

(U) A Physical and Numerical Study of Three-Dimensional Skewed Mixing Layers

5. FUNDING NUMBERS

PE - 61102F
PR - 2308
SA - BS
G - AFOSR-91-0374

6. AUTHOR(S)

Sanjiva K. Lele

7. PERFORMING ORGANIZATION NAME(S) AND ADDRESS(ES)

Department of Aeronautics & Astronautics &
Mechanical Engineering
Stanford University
Stanford, CA 94305-4035

AFOSR-TR-96
0847

9. SPONSORING/MONITORING AGENCY NAME(S) AND ADDRESS(ES)

AFOSR/NA
110 Duncan Avenue, Suite B115
Bolling AFB, DC 20332-0001

NA

10. SPONSORING/MONITORING AGENCY REPORT NUMBER

91-0374

11. SUPPLEMENTARY NOTES

12a. DISTRIBUTION/AVAILABILITY STATEMENT

Approved for public release; distribution is unlimited

19960523 203

13. ABSTRACT (Maximum 200 words)

The effect of skewing the two free-streams on the development of a compressible mixing layer was studied. The results of stability analysis show that skewing has the simultaneous effect of increasing the effective velocity ratio, which is a destabilizing effect, and increasing the effective convective Mach number, which is a stabilizing effect.

Direct numerical simulations of a spatially-evolving mixing layer with equal velocity magnitude but skewed in opposite directions were conducted to study the non-linear evolution. Three skewing angles were considered: 30°, 60°, and 90°. For the low skewing angle cases, the mixing layer rolls up and forms a pattern of streamwise vortices. For the 90° case, vortex breakdown was observed, which significantly enhances the mixing. For high Mach numbers, oblique waves are more unstable which form a pattern of streamwise vortices with increasing spanwise undulation.

The skewing effect can be practically realized by adding swirl to a circular mixing layer. Results of stability analysis show that adding a small amount of swirl near the center of the mixing layer significantly enhances the maximum amplification rate, and the enhancement sustains under compressible conditions. The disturbance energy budget shows that a significant of disturbance energy is extracted from the shear in the swirl component.

14. SUBJECT TERMS	15. NUMBER OF PAGES
compressible mixing layers, mixing enhancement, shear layers, compressible turbulence	20
	16. PRICE CODE

17. SECURITY CLASSIFICATION OF REPORT	18. SECURITY CLASSIFICATION OF THIS PAGE	19. SECURITY CLASSIFICATION OF ABSTRACT	20. LIMITATION OF ABSTRACT
Unclassified	Unclassified	Unclassified	UL

Final Report on

A Physical and Numerical Study of Three- dimensional Skewed Mixing Layers

for the period 8/15/91 – 11/14/95

by
Sanjiva K. Lele
Dept. of Mechanical Engineering
Stanford University, Stanford, CA 94305-4035

Supported by

Air Force Office of Scientific Research

under grant AFOSR-91-0374
Contract Monitor Dr. J. McMichael

Final Report on

A Physical and Numerical Study of Three- dimensional Skewed Mixing Layers

for the period 8/15/91 - 11/14/95

by

Sanjiva K. Lele
Dept. of Mechanical Engineering
Stanford University, Stanford, CA 94305-4035.

Summary

This report summarizes the findings of the research conducted under grant AFOSR-91-0374 from the Air Force Office of Scientific Research, Air Force Materiel Command, USAF. The bulk of the research effort pertains to the original topic of skewed compressible mixing layers. This research is summarized in the main report to follow. Research was also initiated, during the last year of the grant period, on a second topic dealing with the instability of curved compressible mixing layers. Results from this effort are summarized in the appendix to the main report.

FINAL REPORT
A NUMERICAL INVESTIGATION OF SKEWED MIXING LAYERS

Sanjiva K. Lele and Ganyu Lu
Mechanical Engineering Department, Stanford University
Stanford, California 94305

1 Introduction

A mixing layer as a prototypical simple flow is of fundamental importance in industrial applications. Detailed understanding of the physics of compressible mixing layers is essential in developing new turbulence and mixing models. Recent interest in high-speed flow and supersonic combustion ram jet (scramjet) has been motivating the study of compressible mixing layers. In a scramjet engine the time taken to mix the fuel and oxidizer is very short and must occur within the combustion chamber for the heat release to generate thrust. However, experimental and computational studies have shown that mixing layer flows become more stable under highly compressible conditions. The reduced mixing, in turn, can cause inefficient combustion in the scramjet engine and other propulsion systems. Good mixing between the two streams is crucial in designing these systems.

In many practical situations a mixing layer is more complex than the frequently studied idealization of a plane mixing layer. For example, the initial spreading of a swirling jet involves three-dimensional mixing layers. In the separated flow over a leading edge of a slender delta wing at incidence, the flow separates near the leading edge and forms a mixing layer with non-parallel streams. This mixing layer rolls up into a core of high vorticity (Hall 1966). In the flow field arising in a lobed mixer where the upper and lower streams are alternatively turned into the lobed troughs, the two streams are locally non-parallel and form an array of counter-rotating streamwise vortices near the mixer. Most three-dimensional boundary layer separations involve complex mixing layers. In these practical flows, however, the effects of pressure gradients, flow curvature and three-dimensional mean flow occur simultaneously, making it difficult to interpret the individual effects. A skewed mixing layer, i.e. mixing layer between two streams of different directions and velocity magnitudes, allows a study of the skewing effect in isolation.

Skewing the two streams can enhance the mixing. This effect was observed in experiments (Hackett & Cox 1970; Gründel & Fiedler 1992; Fric 1995) and in linear stability analyses (Grosch & Jackson 1991; Lu & Lele 1993a, 1993b). This work aims to understand the mechanism of mixing enhancement by skewing and offers parameters which can be used to assess the skewing effect. The effect of adding swirl to a circular mixing layer, as an example for the practical realization of the skewing effect, is also studied by means of stability analysis. This project focused on the following questions:

(1) What is the effect of skewing on the incompressible mixing layers?

(2) Will the same effect be sustained in compressible mixing layers? What is the compressibility effect?

(3) What is the effect of skewing on the vortical structures that develop in the mixing layer?

(4) How can the skewing effect be exploited in a practical geometry?

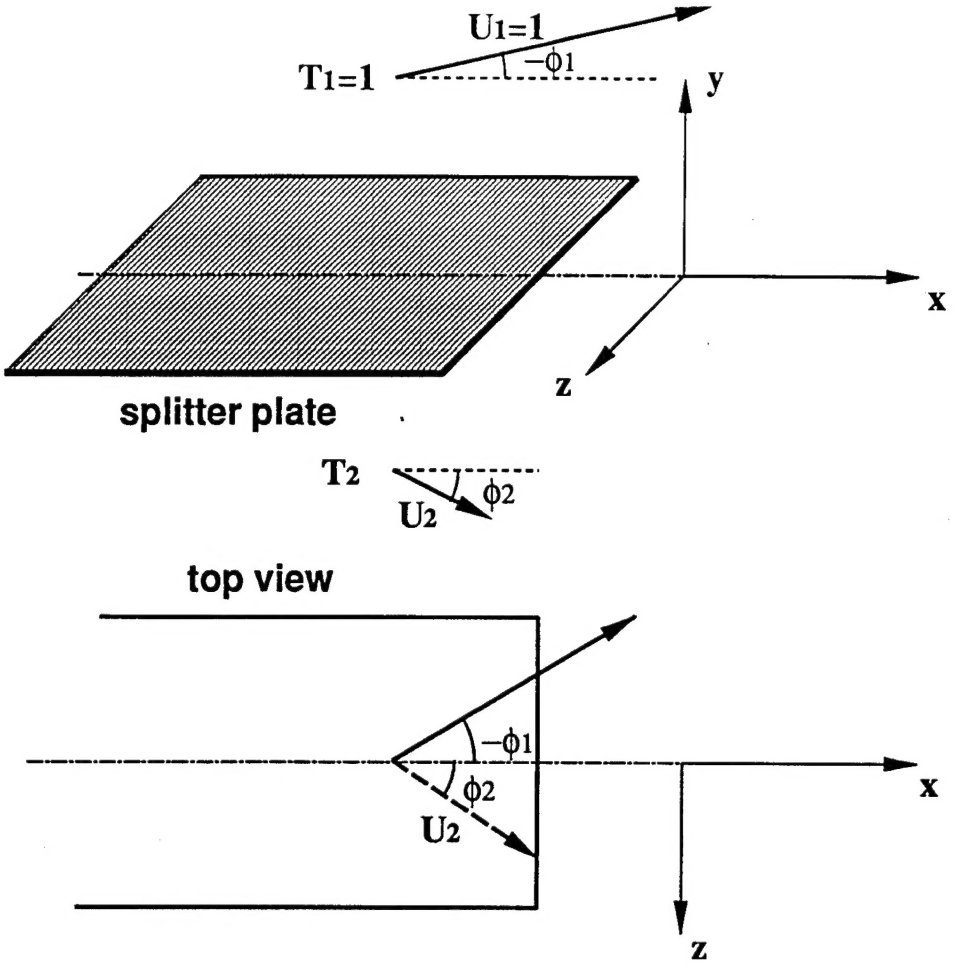

Figure 1: Schematic of a skewed mixing layer.

2 Linear Stability Analysis

A skewed compressible mixing layer is the shear layer between two streams of different velocity magnitudes and directions and, in general, different temperatures (Figure 1). The Cartesian coordinates (x, y, z) are chosen so that the y-coordinate is normal to the layer and the z-coordinate is along an assumed homogeneous direction for the mean flow. The x-direction is also called the streamwise direction, and the z-direction the spanwise direction. Physically the homogeneous direction spans across a splitter plate which separates the two free-streams. The mean pressure is assumed to be uniform and the fluid is taken to be a perfect gas with constant specific heats.

The mean flow is governed by the three-dimensional boundary-layer equations and can be reduced to the sum of a two-dimensional shear flow and a uniform flow.

The flow variable can be decomposed into its mean and a disturbance:

$$f = \bar{f} + \text{Real}\left\{\hat{f}(y)\exp[\mathrm{i}(\alpha x + \beta y - \omega t)]\right\} \quad (1)$$

where the overbar denotes a mean quantity, which is taken from the similarity solutions. In the equation, $\hat{f}$ is the complex eigenfunction depending only on y, ω is the frequency, and α and β are the wavenumbers in the streamwise (x) and spanwise (z) directions respectively. In the spatial problem, disturbances grow in space and not in time, so ω is real and both α and β are complex for a general perturbation. The imaginary parts of wavenumbers can be re-expressed in terms of

the spatial amplification rate κ and the amplification angle σ

$$\alpha_i = -\kappa \cos\sigma, \qquad \beta_i = -\kappa \sin\sigma \tag{2}$$

The subscripts i denote the imaginary part of a complex number.

In a skewed mixing layer, the existence of the cross flow ($\bar{w} \neq 0$) makes the mean flow three-dimensional. The splitter plate edge, due to its receptivity behavior, may introduce disturbances which are periodic in the z-direction. In this case the disturbances do not amplify for $z \to \pm\infty$ or $\sigma = 0$. Therefore, the spatial amplification rate is $-\alpha_i$. If $-\alpha_i > 0$ and Briggs' criterion for amplifying waves (Briggs 1964) is satisfied, the disturbance is spatially amplifying. Further downstream of the splitter plate, this assumption ($\sigma = 0$) does not necessarily hold. From the study of asymptotic growth of disturbances from a spatially compact source (Lu & Lele 1993b), we found that the disturbances grow along the mean convection direction, which will be defined later. Therefore, in this study we align the convection direction with the x-direction in the mean flow, so that the stability analysis results are valid in both near and far field.

From both experiments and linear stability analysis it was found that the growth rate of a plane mixing layer can be estimated by using simple combinations of the free-stream quantities. Such parameters are defined below and their effectiveness to scale the maximum amplification rate of the skewed mixing layer is demonstrated.

For plane incompressible mixing layers, the convection velocity U_c can be estimated by

$$U_c = \frac{\sqrt{T_2} + U_2}{\sqrt{T_2} + 1} \tag{3}$$

and the growth rate of a plane mixing layer can be estimated by the ratio of the velocity difference ΔU to the convection velocity U_c

$$\lambda = \frac{\Delta U}{U_c} = \frac{(1 - U_2)(\sqrt{T_2} + 1)}{\sqrt{T_2} + U_2} \tag{4}$$

For skewed mixing layers, the convection velocity (U_c, W_c) can be similarly estimated by

$$U_c = \frac{\sqrt{T_2}\cos\phi_1 + U_2 \cos\phi_2}{\sqrt{T_2} + 1} \tag{5}$$

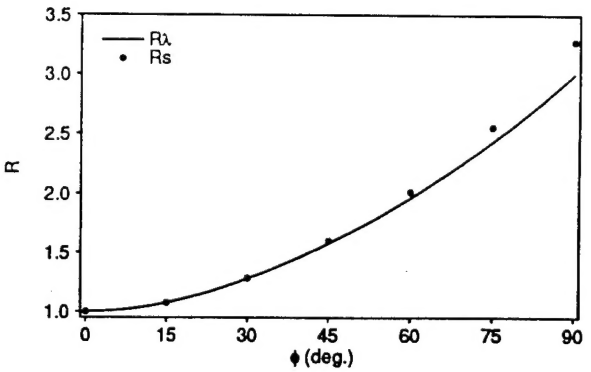

Figure 2: Comparison of the normalized maximum amplification rate R_S with the normalized effective velocity ratio R_λ as a function of the skewing angle ϕ for incompressible skewed mixing layer with $U_2 = 0.5$ and $T_2 = 1$.

$$W_c = \frac{\sqrt{T_2}\sin\phi_1 + U_2 \sin\phi_2}{\sqrt{T_2} + 1} \tag{6}$$

The velocity difference is that of the effective shear given by

$$\Delta U = \sqrt{1 - 2U_2\cos\phi + U_2^2} \tag{7}$$

The effective velocity ratio may be defined as

$$\lambda = \frac{\Delta U}{U_c \cos\sigma + W_c \sin\sigma} \tag{8}$$

where σ is the direction of growth. If we require $W_c = 0$, i.e. the mean convection direction is aligned in the x direction, then it follows from (6) that

$$\tan\phi_1 = -\frac{U_2 \sin\phi}{\sqrt{T_2} + U_2\cos\phi} \tag{9}$$

This is different from our earlier work reported in Lu & Lele (1993) where $\phi_1 = 0$ was used and results were restricted to $\sigma = 0$. For the present mean flow, σ is naturally zero. The number of degrees of freedom is reduced to two: ω and θ. The effective velocity ratio is compared with the maximum amplification rate from the stability analysis of the incompressible mixing layers in Figure 2. For results presented, $U_2 = 0.5$, $T_2 = 1$ and $M_1 = 0$. In this figure the skewing effect on the

amplification rate is isolated by plotting the maximum amplification rate, which is normalized using the corresponding value of an unskewed mixing layer with the same Mach number, velocity ratio and temperature ratio:

$$R_S = \frac{|\alpha_i|_{\max}(M_1, U_2, T_2, \phi)}{|\alpha_i|_{\max}(M_1, U_2, T_2, 0)} \qquad (10)$$

Figure 2 also shows the normalized effective velocity ratio R_λ, normalized in the same way as (10). The maximum amplification rate increases with the skewing angle. The maximum amplification rate is proportional to the effective velocity ratio. The increase in the maximum amplification rate with skewing can thus be estimated from the increase in the effective velocity ratio. Results for different velocity ratio and temperature ratio also show similar agreement (Lu & Lele 1993a).

The free-stream Mach number M_1 does not provide a good measure of the compressibility in mixing layer. It is the velocity difference between the two streams that matters. The decomposition of the mean flow into the sum of a uniform flow and a two-dimensional shear flow leads to the definition of the effective convective Mach number for the skewed mixing layer as the convective Mach number of the effective shear. The definition of a convective Mach number which is frequently used for a plane mixing layer is (for $\gamma_1 = \gamma_2$)

$$M_C = \frac{\Delta\tilde{U}_2}{a_1 + a_2} = \frac{\sqrt{1 - 2U_2\cos\phi + U_2^2}}{1 + \sqrt{T_2}} M_1 \qquad (11)$$

where a_1 and a_2 are the sound speeds of the fast-moving and slow-moving streams respectively. This definition was used to collapse the available growth rate data from experiments (Bogdanoff 1983; Papamoschou & Roshko 1988; also see Dimotakis 1991 for a review). Sandham and Reynolds (1990) also use this definition to rescale their linear stability results.

For compressible mixing layers, when the skewing angle increases, although the free-stream Mach number is fixed, the effective convective Mach number M_C is increased. Since compressibility stabilizes the mixing layer, the skewing ef-

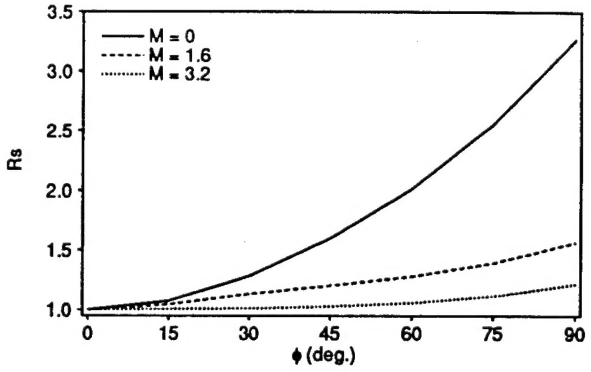

Figure 3: The normalized maximum amplification rate R_S as a function of the skewing angle ϕ for skewed mixing layer with $U_2 = 0.5$, $T_2 = 1$ and different Mach numbers.

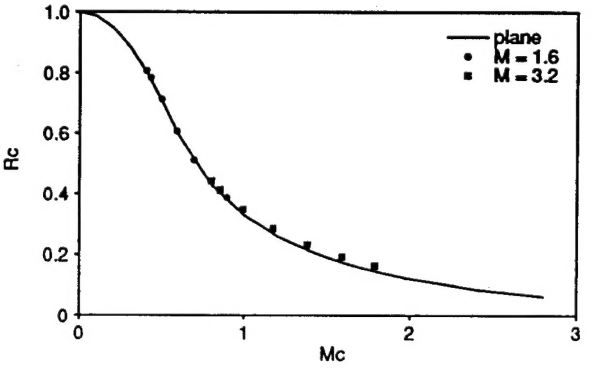

Figure 4: The normalized maximum amplification rate R_C as a function of the effective convective Mach number M_C for skewed mixing layer with $U_2 = 0.5$, $T_2 = 1$ and different Mach numbers. (Solid line is the normalized maximum amplification rate of the plane compressible mixing layer with $U_2 = 0.5$, $T_2 = 1$.)

fect on the amplification rate is expected to decrease.

Figure 3 shows the normalized maximum amplification rate R_S as a function of the skewing angle ϕ for $U_2 = 0.5$, $T_2 = 1$ and $M_1 = 0$, 1.6 and 3.2. For compressible mixing layers, skewing still increase the maximum amplification rate, but the enhancement is decreased as the free-stream Mach number M_1 is increased.

To scale this compressibility effect, the maximum amplification rate of the compressible skewed mixing layer is normalized using the results from the corresponding incompressible skewed mixing layer

$$R_C = \frac{|\alpha_i|_{max}(M_1, U_2, T_2, \phi)}{|\alpha_i|_{max}(0, U_2, T_2, \phi)} = R_C(M_C) \quad (12)$$

Figure 4 shows the normalized amplification rate R_C of the compressible skewed mixing layer as a function of the effective convective Mach number M_C for $U_2 = 0.5$ and $T_2 = 1$ and different Mach number M_1. All data collapse to the values of the plane compressible mixing layers (shown by the solid line), indicating that the scaling (12) is successful. The compressibility effect on skewed mixing layers can be scaled using the effective convective Mach number as the single parameter.

Since skewed mixing layers are three-dimensional in nature, the assumption that the disturbances grow along the mean convection direction, which is also chosen as the streamwise x-direction, needs to be verified. Disturbances arising from a time-harmonic spatially-compact source are studied. The asymptotic growth for large x is analysed using the saddle point method. The skewed mixing layers are compared with the corresponding unskewed mixing layers. Disturbances arising from a spatially-compact source grow in a wedge-shaped region centered at the mean convection direction. This justifies the assumption that the disturbances grow in the convection direction. Detailed results from this analysis can be found in Lu & Lele (1996).

3 Direct Numerical Simulations

Direct numerical simulations of the three-dimensional compressible Navier-Stokes equations are conducted. A particular subset of the skewed compressible mixing layers is studied in detail: the mixing layer between two streams with equal velocity magnitudes but skewed in opposite directions. To assess the skewing effect, we compare results for different skewing angles while fixing other mean flow parameters.

Time advancement is explicit and carried out by a compact-storage third-order Runge-Kutta scheme (Wray 1986). Only two storage locations are needed for each substep, and three evaluations of the right hand side of the equations are needed.

The spatial derivatives are discretized with the sixth order Padé finite difference scheme (Lele 1992). Thompson's non-reflecting boundary conditions (Thompson 1987,1990) are used in the inhomogeneous directions (x- and y-directions). The code is written in the VECTORAL language (Wray 1988), and implemented on the Cray Y-MP C90 at NASA-Ames Research Center.

The laminar compressible boundary-layer solutions show that the u-velocity is uniform, which is also the mean convection velocity U_C, and the effective shear is along the spanwise z-direction The inviscid stability analysis shows that a stationary spanwise (z) wave is the most unstable wave for low convective Mach numbers. The instability wave grows along the mean convection direction due to the shear instability, and the non-linear evolution (roll-up) of the disturbance forms a pattern of streamwise (x) vortices. The existence of subharmonic wave makes neighboring fundamental vortices to undergo a pairing process to form streamwise vortices of a larger scale. Such helical vortex structures have been observed in the flow visualizations of incompressible skewed mixing layers conducted by Gründel & Fiedler (1992). For high convective Mach number, a pair of oblique waves is most unstable. A pair of horseshoe vortices was observed to develop in a temporal simulation by

Table 1: Simulation parameters

ϕ	M_1	λ	M_C	$\lvert\alpha_i\rvert_{\text{fun}}$	$\lvert\alpha_i\rvert_{\text{sub}}$	L_z	L_x	A_{fun}	A_{sub}	mesh size
30°	0.6	0.54	0.16	0.10	0.08	7.85	80	0.01	0	$251 \times 189 \times 65$
30°	0.6	0.54	0.16	0.10	0.08	14.7	100	0.01	0.01	$251 \times 189 \times 81$
60°	0.6	1.16	0.30	0.20	0.15	7.85	65	0.02	0	$251 \times 189 \times 65$
90°	0.6	2.00	0.42	0.31	0.23	7.85	50	0.05	0	$251 \times 189 \times 65$
90°	0.6	2.00	0.42	0.31	0.23	14.7	60	0.03	0.01	$241 \times 189 \times 81$
90°	0.6	2.00	0.42	0.31	0.23	14.7	80	0.03	0.03	$341 \times 189 \times 81$
90°	1.2	2.00	0.83	0.16		14.7	60	0.02		$251 \times 189 \times 81$

Sandham & Reynolds (1989). In the high Mach number skewed mixing layer considered here, a pair of streamwise vortices with increasing spanwise undulation forms.

The boundary layer solutions are used as mean flow profiles at the inflow. Perturbations are added at the inflow in the form of eigenfunctions of unstable waves from linear inviscid stability analysis.

Three skewing angles are selected for detailed studies, i.e. $\phi = 30°$, $60°$ and $90°$. The related parameters are shown in Table 1. A free-stream Mach number $M = 0.6$ is chosen for the low compressibility cases. The temperatures of the two streams are the same: $T_2 = 1$. The Reynolds number is chosen small enough so that the flow can be fully resolved and large enough to capture the inviscid nature of the instability. From previous experience on direct simulations of plane mixing layers the Reynolds number is 500 based on the inflow vorticity thickness and mean free-stream velocity. The Prandtl number is constant and chosen as 0.7, and the Schmidt number for the passive scalar is unity. As the skewing angle increases, the amplification rate of the most unstable wave $|\alpha_i|_{\text{max}}$ also increases and is proportional to the effective velocity ratio λ (Table 1). The domain width L_z, which matches the wavelength of the most unstable wave, is used. For $A_{\text{sub}} \neq 0$, the domain size L_z contains one wave length of the subharmonic. The wavenumbers β for the most unstable waves for $M_1 = 0.6$ occur to be approximately the same for different skewing angles, while for $M_1 = 1.2$, β is approximately half as much as those for $M_1 = 0.6$. The streamwise length of the simulation domain L_x is also shown in the table; it is chosen to allow the spatial development of the vortical structures to be completed within the computational domain. The transverse length of the simulation domain L_y is the same for all cases and equal to 18 times the inflow vorticity thickness. Doubling the free-stream Mach number to $M = 1.2$ allows a study of the compressibility effect, which is the last case in Table 1. More details of the numerical method can be found in Lu & Lele (1996).

Since stationary spanwise wave (the most unstable wave) is used as the inflow perturbation, the inflow conditions do not force unsteady perturbations and a steady state is expected downstream. Figure 5 shows the time history of pressure at different x-locations along the center of the vortex core. The flow field is initialized using the same eigenfunctions as those used in the inflow perturbation without accounting for any spatial amplification. In the early stage the flow downstream evolves in time. At any given x-station, the flow remains unaltered until spatially-amplified disturbance reaches the chosen station. Near the inflow the pressure monotonically decreases, reaching its steady state. Downstream the pressure decreases at the beginning and then increases to its steady state. The u-velocity decreases a small amount and then increases and successively becomes constant. The whole flow field reaches a steady state after an initial transient of less than one and a half flow-through times (one flow-through time equals

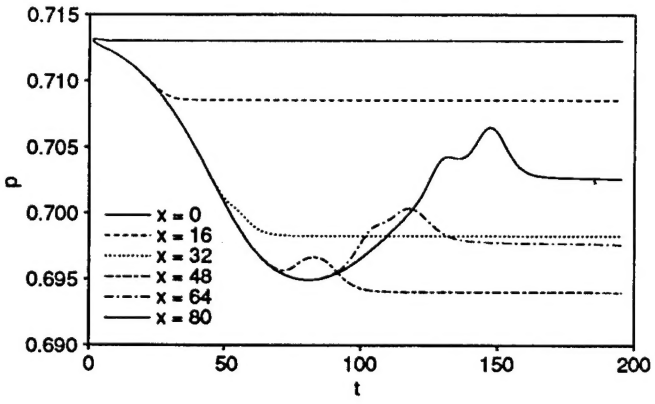

Figure 5: Time history of pressure at different x-locations of the center of the streamwise vortex core for $M = 0.6$ and $\phi = 30°$ with only fundamental disturbance.

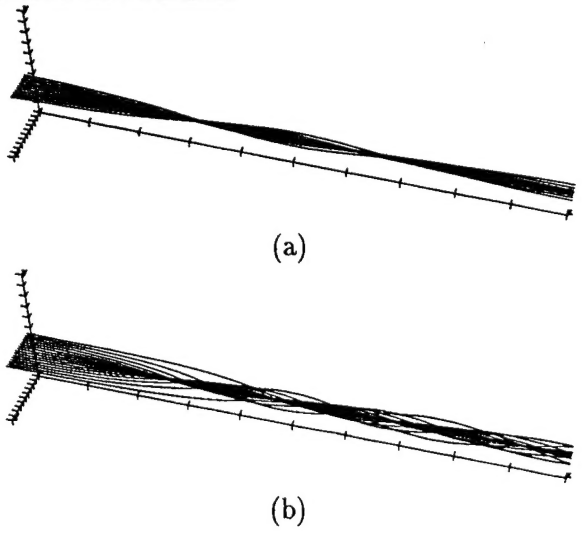

Figure 6: Vortex lines (a) and streamlines (b) for $M = 0.6$ and $\phi = 30°$ with only fundamental disturbance. (Tic marks in x, y and z are at 8, 2 and 1 δ_{ω_0} intervals.)

138). The following results are at the steady state.

The overall vortical structure for the 30° skewing case is shown in Figure 6 with vortex lines and streamlines starting from the inflow plane at $y = 0$. As the disturbance grows due to the shear instability, the streamwise vorticity is collected into a streamwise roller. The layer of vorticity at the inflow rolls up, and forms a round streamwise roller. The effective shear, which is along the z-direction, makes the roller elliptic. The vortex lines and streamlines are helically twisted along with the roll-up of the mixing layer in the (y, z)-plane. Due to the periodic boundary condition in the z-direction, the single vortex core, in fact, represents a spanwise periodic pattern of streamwise vortices.

At large skewing angles, the cross-shear velocity difference is larger than the mean convection velocity, so the associated streamwise vorticity is strong. Figure 7 shows some vortex lines and streamlines starting from the inflow plane at $y = 0$. For some distance downstream of the inflow the vortex lines and streamlines are helically twisted similar to the lower skewing angle cases, except that the twisting is much faster. Beyond a particular x-location, instead of continuing the twisting, the concentrated vortex tube suddenly bulges out, suggesting that vortex breakdown has occurred. Inside the breakdown bubble, the vorticity is very small. Downstream of the breakdown, the streamlines stop twisting and become straight.

Figure 8 shows the time history of pressure at different x-locations for the 90° case. The flow through time for this case is 59, and the simulation has gone through about four flow through times. The flow reaches a steady state upstream of the vortex breakdown. Downstream of the breakdown the flow is unsteady.

From stability analysis, we know that skewing the two streams increases the maximum amplification rate. The mixing layer growth rate can be measured using the momentum thickness. Figure 9(a) shows the momentum thickness δ_m as a function of x for $\phi = 30°$, 60° and 90°. As the skewing angle increases, the spreading rate in the momentum thickness is significantly enhanced. For the

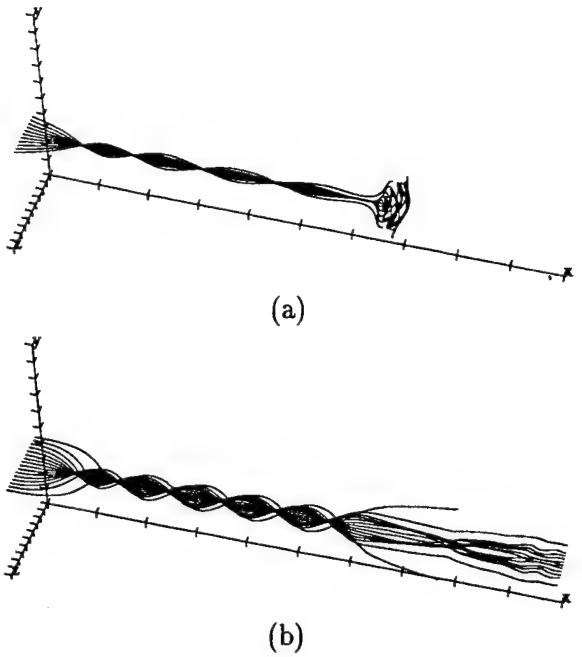

Figure 7: Vortex lines (a) and streamlines (b) for $M = 0.6$ and $\phi = 90°$ with only fundamental disturbance. (Tic marks in x, y and z are at 5, 2 and 1 δ_{ω_0} intervals.)

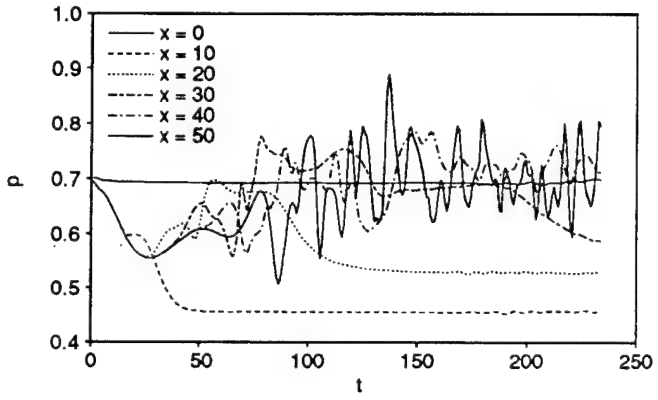

Figure 8: Time history of pressure at different x-locations of the center of the streamwise vortex core for $M = 0.6$ and $\phi = 90°$ with only fundamental disturbance.

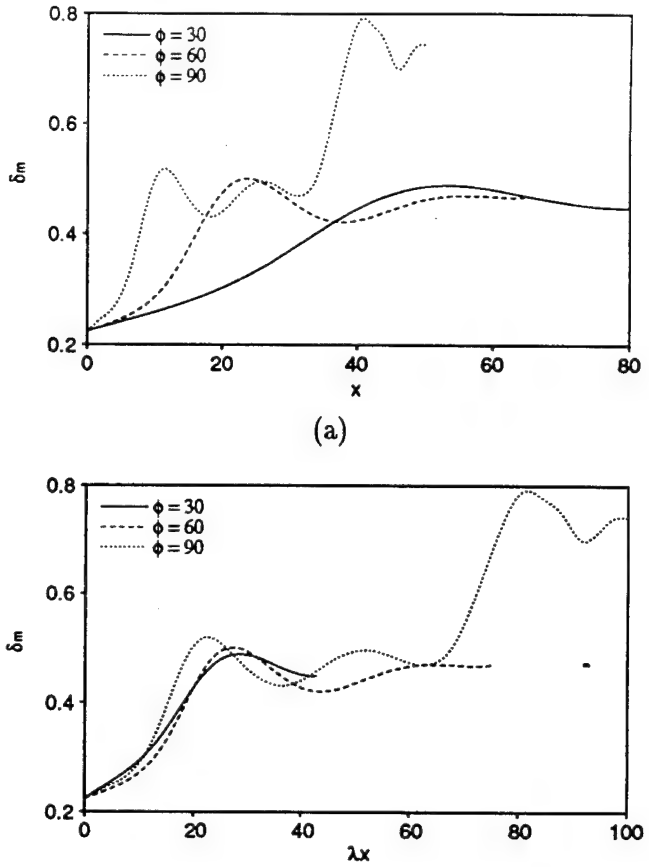

Figure 9: Momentum thickness as a function of x (a) and λx (b) for $M = 0.6$ and different skewing angles with only fundamental disturbance.

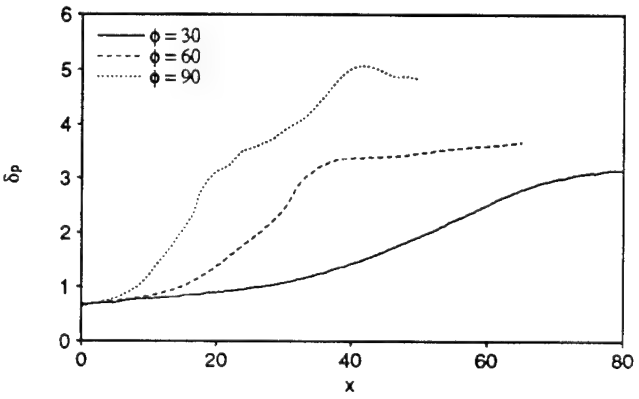

Figure 10: Product thickness with $C_2 = 0.2$ and $C_1 = 0.8$ for $M = 0.6$ and different skewing angles with only fundamental disturbance.

90° case, the second jump in δ_m corresponds to the vortex breakdown. The increase in spreading rate due to skewing is primarily due to the increased effective velocity ratio λ. This is demonstrated in Figure 9(b) by plotting the momentum thickness δ_{m_z} against x times λ, which effectively collapses the three curves. The increase due to vortex breakdown remains unaccounted in this scaling.

A measure of the mixing between the two streams is the product thickness calculated from a conserved passive scalar with value 0 and 1 in the lower and upper free-streams. The product thickness is defined as

$$\delta_p = \frac{\text{area}(C_2 < c < C_1)}{L_z} \tag{13}$$

where area$(C_2 < c < C_1)$ is the area on the (y, z)-plane where c has a value between C_2 and C_1. The (y, z)-plane is divided into small cells centered at the nodes. The area$(C_2 < c < C_1)$ is computed by summing the areas of the cells whose nodes satisfy the condition $C_2 < c < C_1$. A comparison of the product thickness among the three cases is shown in Figure 10. Skewing increases the growth rate of the product thickness.

To assess the effect of the vortex breakdown on the mixing, we compare the 90° case to the corresponding two-dimensional temporal simulation, which forces the vortex breakdown not to occur. Figure 11 shows the comparison of the momentum thickness and product thickness, while the temporal evolution is converted to the spatial evolution using the mean convection velocity. Near the inflow the two curves agree. Beyond $x = 30$ the spatial evolution differs markedly from the temporal case. As is evident from Figure 11, the vortex breakdown significantly enhances the mixing.

Other DNS cases which explore the impact of the subharmonic disturbances on the nonlinear growth, and the high compressibility case are reported in Lu & Lele (1996). The existence of the subharmonic waves makes the streamwise vortices undergo a helical pairing process and form vortices of larger size. For high Mach numbers, oblique waves are more unstable which form a pattern of streamwise vortices with increasing

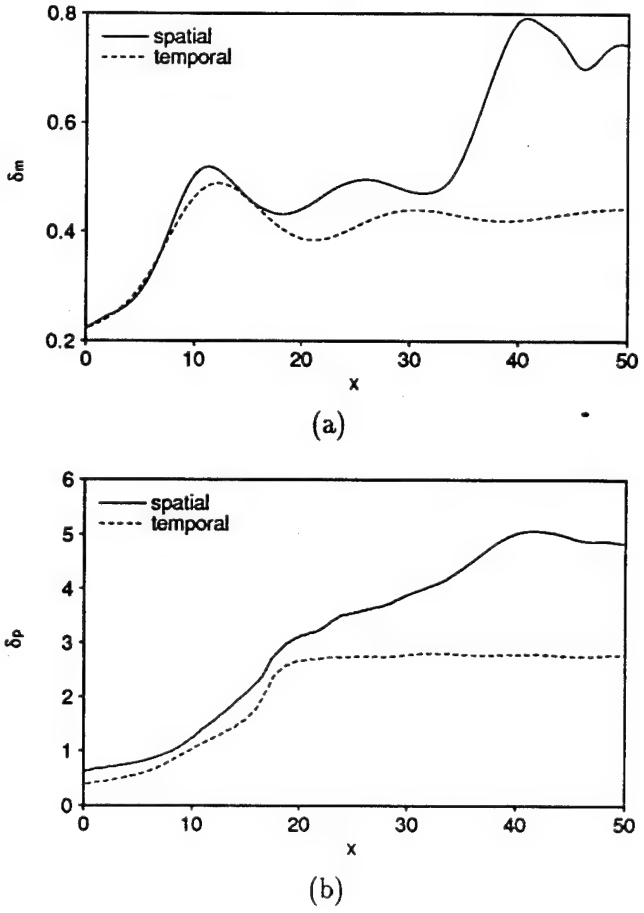

Figure 11: Comparison between the spatial simulation and the corresponding temporal simulation for $M = 0.6$ and $\phi = 90°$ with only fundamental disturbance: (a) momentum thickness (b) product thickness with $C_2 = 0.2$ and $C_1 = 0.8$.

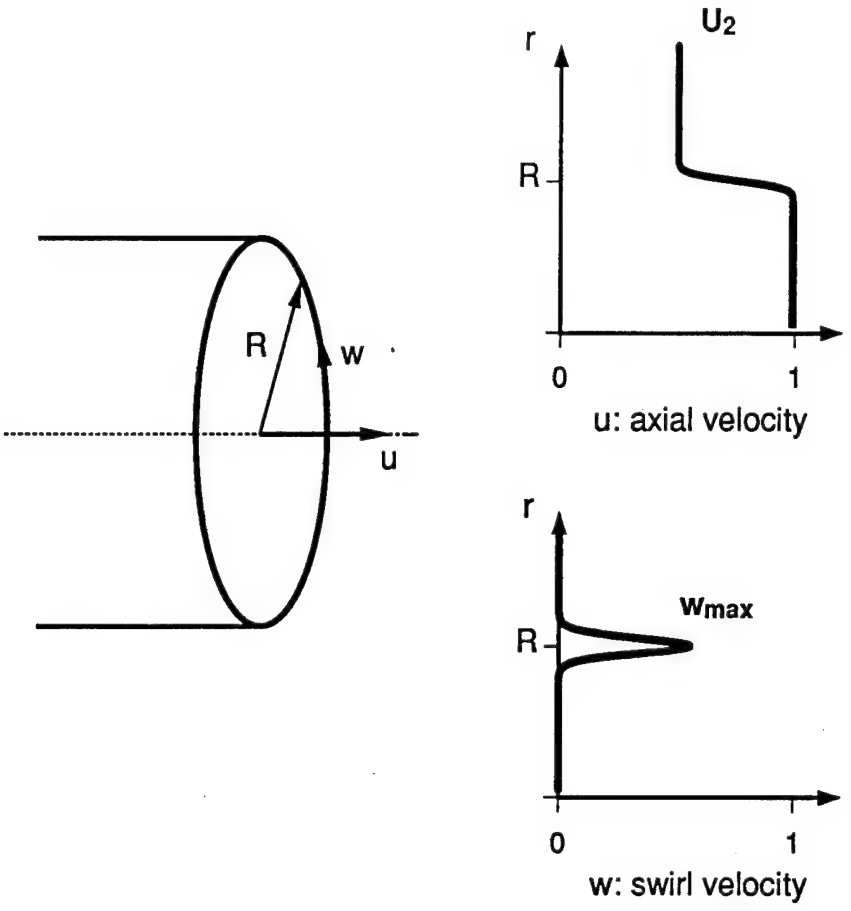

Figure 12: Schematic of a swirling mixing layer.

spanwise undulation in the non-linear regime.

4 Swirling Mixing Layer

An experimental realization of skewed mixing layers requires a wide splitter plate. Even then the overlying portion of the two skewed streams decreases laterally as the flow proceeds downstream. A configuration which avoids this difficulty is a circular mixing layer. A swirl component is added within the mixing layer, as shown in Figure 12. This can be realized in experiments by turning vanes of small height affecting only the boundary layer of a jet nozzle. Unlike skewed mixing layers, the swirling mixing layer contains a cross flow component in form of the the swirl velocity, which decays on both sides, and there are two inflection points in the mean profile of the swirl component. The peak value of the swirl component decreases downstream by viscous diffusion and due to nonlinearity. The mean flow is solved numerically using the compressible boundary-layer equations in cylindrical coordinates. Stability analysis is performed on the mean flow to study the effect of swirl.

The cylindrical coordinates (x, r, θ) are chosen so that the mixing layer flows along the x-direction, and r and θ are the radial and azimuthal coordinates respectively.

The numerical method to solve the mean flow boundary-layer equations is adopted from Anderson, Tannehill & Pletcher (1984). Due to

Table 2: Parameters for the stability analysis of swirling mixing layers. Note values at the spatial location x listed in the table are used to define the non-dimensional parameters.

case	M_1	$w_{\max}$	R	δ_S	S	$\psi_{\max}$
M00W00	0	0	10		0	0°
M00W25	0	0.25	10	1	0.05	19°
M00W50	0	0.50	10	0.98	0.11	35°
M00W40	0	0.40	8	0.98	0.09	29°
M00DS2	0	0.49	10	2	0.22	36°
M16W00	1.6	0	10		0	0°
M16W55	1.6	0.55	10	0.96	0.11	37°
M32W00	3.2	0	10		0	0°
M32W57	3.2	0.57	10	0.94	0.13	40°

the parabolic nature of the equations, x can be treated as the advancing variable. The Crank-Nicholson method is used, which has second-order accuracy with respect to both independent variables x and r.

The mean flow parameters of swirling mixing layers include: the radius of the round mixing layer R, the thickness of the swirl δ_S, the maximum azimuthal velocity $w_{\max}$, the Mach number M_1, the velocity ratio U_2 and the temperature ratio T_2. In all cases reported here, $U_2 = 0.5$ and $T_2 = 1$. To keep the curvature effect small, the radius R at the reference station is chosen as 20.

The flow variables can be decomposed into their means and a disturbance:

$$f = \bar{f} + \text{Real}\left\{\hat{f}(r)\exp[\mathrm{i}(kx + m\theta - \omega t)]\right\} \quad (14)$$

where k the streamwise wave number, and m the azimuthal mode number and should be an integer. Spatial stability problem is considered here, where k is complex with $-k_\mathrm{i}$ the amplification rate.

Table 2 lists the mean flow parameters used in the stability analysis. The degree of swirl can be characterized by the swirl number

$$S = \frac{\int_0^\infty \rho u w r^2 \mathrm{d}r}{R\int_0^\infty \rho\left(u^2 - \frac{1}{2}w^2\right) r\mathrm{d}r} \quad (15)$$

However, if there is coflow or $U_2 \neq 0$, the integral in the denominator is infinite. Using $u - U_2$ to substitute u in (15) could avoid the difficulty. Another assessment of the degree of swirl is the helix angle of the velocity vector relative to the x-axis

$$\psi = \tan^{-1}\left(\frac{w}{u}\right) \quad (16)$$

This angle compares the local swirl velocity and axial velocity. The thickness of swirl δ_S is comparable with the vorticity thickness of the mixing layer unless otherwise specified. The magnitude of swirl velocity is basically described by a single parameter $w_{\max}$. In the stability analysis, the mean flow obtained from the numerical solutions of the boundary-layer equations are fitted with a cubic spline interpolation. All the mean flow profiles can be found in Lu & Lele (1996).

The results for a non-swirling incompressible mixing layer, which serves as the baseline case, is shown in Figure 13 with the spatial amplification rate $-k_\mathrm{i}$ as a function of the frequency ω for different m. The spatial amplification rate $-k_\mathrm{i}$ has maximum value at $m = 0$, which is an axisymmetric mode. Overall $-k_\mathrm{i}$ decreases as m increases. This is similar to plane mixing layer where two-dimensional disturbances are more unstable than oblique disturbances. All values of m were tracked in the stability problem. Only a sample of these are plotted for clarity.

Increasing swirl ($w_{\max} = 0.5$) yields results shown in Figure 14. The amplification rate $-k_\mathrm{i}$ is enhanced further for small m. The most unstable wave occurs at $m = 17$ and its frequency is small. The unstable frequency region moves towards negative frequencies, which implies that disturbances with negative frequencies are more unstable.

For non-swirling incompressible mixing layer, shear instability in the axial velocity is the only mechanism for disturbance growth. For swirling mixing layer, the azimuthal velocity w increases and then decreases with r. The decrease of rw with r makes the flow centrifugally unstable. This mode is shown in Figure 15. For small amount of swirl, the amplification rate of this mode is smaller than the Kelvin-Helmholtz mode. For larger swirl, the amplification rate of

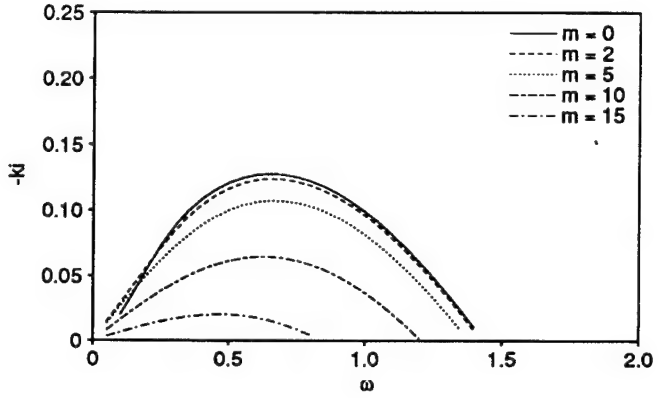

Figure 13: Spatial amplification rate $-k_i$ as a function of frequency ω for non-swirling incompressible mixing layer (Case M00W00: $w_{max} = 0$, $M_1 = 0$ and $R = 10$).

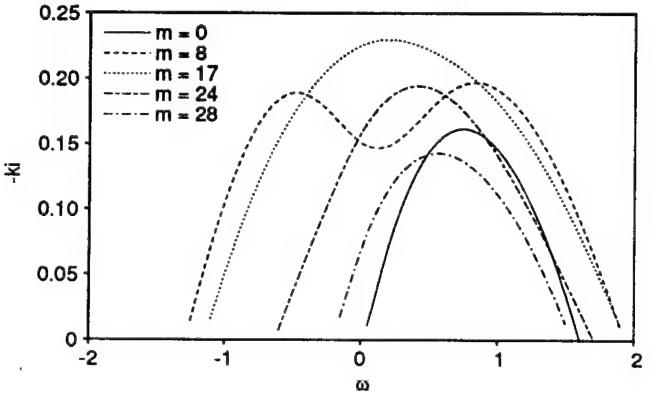

Figure 14: Spatial amplification rate $-k_i$ as a function of frequency ω for swirling incompressible mixing layer (Case M00W50: $w_{max} = 0.50$, $M_1 = 0$ and $R = 10$).

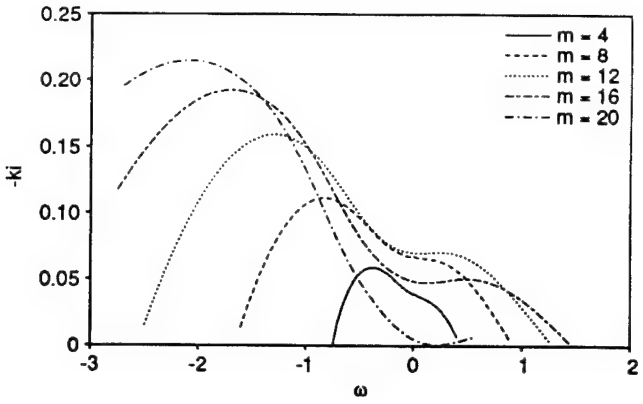

Figure 15: Spatial amplification rate $-k_i$ as a function of frequency ω for swirling incompressible mixing layer (centrifugal mode; Case M00W50: $w_{max} = 0.50$, $M_1 = 0$ and $R = 10$).

the centrifugal mode is comparable to the Kelvin-Helmholtz mode. For the same m, a negative frequency has larger amplification rate than the corresponding positive frequency (same magnitude), indicating that counter-rotating waves are more unstable.

For a free-stream Mach number $M_1 = 3.2$, the convective Mach number is 0.8. A pair of equal and opposite oblique waves is most unstable for a plane mixing layer. Figure 16 shows the spatial amplification rate $-k_i$ as a function of the frequency ω for different m for the non-swirling compressible mixing layer. Helical modes ($m = \pm 4$) becomes most unstable instead of an axisymmetric mode ($m = 0$), which is similar to the behavior in plane mixing layers. Also note that the maximum amplification rate is significantly smaller than the corresponding incompressible case. Adding similar amount of swirl ($w_{max} = 0.57$), Figure 17 shows the spatial amplification rate $-k_i$ as a function of the frequency ω for different m for the swirling compressible mixing layer. Although the maximum amplification rate is somewhat smaller than the corresponding incompressible case, it is much larger than the corresponding non-swirling compressible case. In contrast, at this Mach number skewing has almost no effect on the maximum amplification rate.

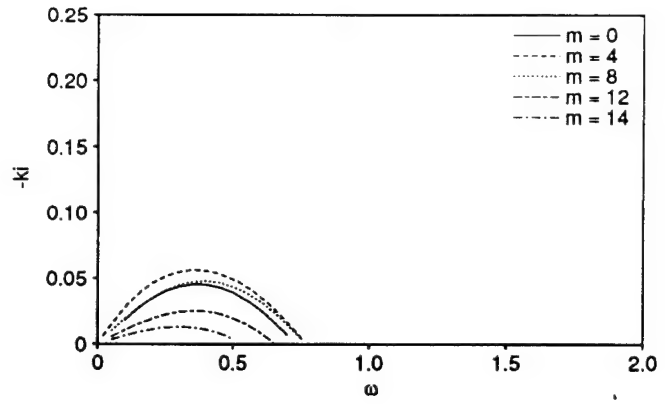

Figure 16: Spatial amplification rate $-k_i$ as a function of frequency ω for non-swirling incompressible mixing layer (Case M32W00: $w_{max} = 0$, $M_1 = 3.2$ and $R = 10$).

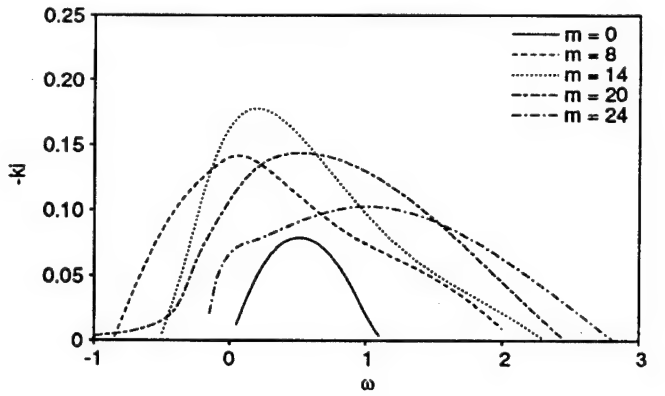

Figure 17: Spatial amplification rate $-k_i$ as a function of frequency ω for swirling incompressible mixing layer (Case M32W57: $w_{max} = 0.57$, $M_1 = 3.2$ and $R = 10$).

5 Conclusions

This work has been concerned with a numerical study of the skewed mixing layer and swirling mixing layer. The methods used were linear inviscid stability analysis and direct numerical simulation of the compressible Navier-Stokes equations. Stability analysis was used to examine the growth of small disturbances. To study the nonlinear behavior, full Navier-Stokes equations were solved. An explicit Runge-Kutta scheme, with the spatial derivative evaluated by a compact sixth-order finite difference scheme was used. A particular subset of skewed mixing layers was simulated: mixing layer between two streams with equal velocity magnitude but skewed in opposite directions. The conclusions from the study are grouped into three main areas: stability analysis of the skewed mixing layer, direct numerical simulations of the skewed mixing layer and stability analysis of the swirling mixing layer.

Stability Analysis of the Skewed Mixing Layer:

- Skewing increases the maximum amplification rate. The enhancement can be scaled by the effective velocity ratio. This concept is derived from the decomposition of the mean flow of the skewed mixing layer into a two-dimensional shear flow (effective shear) plus a uniform flow. The effective velocity ratio is the ratio between the velocity difference in the effective shear and the mean convection velocity.

- For compressible mixing layers, skewing increases the effective velocity ratio, which is a destabilizing effect, and also increases the effective convective Mach number, which is a stabilizing effect. The effective convective Mach number is the Mach number for the effective shear. As a result, the enhancement of the maximum amplification rate by increasing the effective velocity ratio is diminished by the increased effective convective Mach number. The compressibility effect is scaled by the effective convective Mach number.

- The growth of disturbances arising from a spatially-compact time-harmonic source is examined to justify the assumption that the spatial amplification direction is along the mean convection direction. The disturbances from a spatially-compact source grow in a wedge-shaped region centered in the mean convection direction. At low Mach numbers, the propagation direction is close to the effective shear direction, whereas at high Mach numbers, the disturbance propagates in a direction oblique to the effective

shear direction. In both cases the disturbances are amplified along the mean convection direction.

Direct Numerical Simulations of the Skewed Mixing Layer:

- The low Mach number simulations confirm the stability results that the enhancement of the mixing-layer spreading rate can be scaled by the effective velocity ratio. For the particular flow simulated, a stationary spanwise wave is most unstable, which forms a pattern of streamwise vortices. The existence of subharmonic waves makes those streamwise vortices undergo a helical pairing process and form vortices of larger size. For small skewing angle, these vortical structures are comparable to those obtained in a two-dimensional temporally-evolving mixing layer.

- For a large skewing angle, vortex breakdown is observed in the streamwise vortices. Vortex breakdown further enhances the mixing layer spreading rate and the mixing.

- For high Mach numbers, oblique waves are more unstable which form a pattern of streamwise vortices with increasing spanwise undulation in the non-linear regime. The mixing layer spreading rate and mixing measured by the growth of product thickness is reduced. This confirms the stability results that the increased effective convective Mach number stabilizes the flow.

Stability Analysis of the Swirling Mixing Layer:

- Adding the swirl component near the center of a circular mixing layer significantly enhances the maximum amplification rate. In addition to the shear instability of the mixing layer, two additional instability mechanisms are introduced: shear instability in the swirl component, which has two inflection points, and centrifugal instability in the outer part of the swirl component.

- Unlike the skewing effect on compressible mixing layer, the enhancement by adding swirl component sustains under compressible conditions. For the centrifugal mode, the amplification rate is even larger for the compressible flow than the incompressible flow.

- Disturbance energy budget shows that a large part of disturbance energy is extracted from the shear in the swirl component, which can provide only a limited reservoir of energy. Nonlinear simulations are necessary to establish how much growth benefit results from a given amount of swirl.

Publications to date with full support from this grant:

Lu, G. & Lele, S.K. Inviscid instability of a skewed compressible mixing layer, *Journal of Fluid Mechanics*, **249**, 441-463, 1993.

Lu, G. & Lele, S.K. Spatial growth of disturbances in a skewed compressible mixing layer, *AIAA paper*, 93-0214.

Lu, G. & Lele, S.K. Vortex breakdown in skewed compressible mixing layers, *AIAA paper*, 94-0821.

Lu, G. & Lele, S.K. Numerical Investigation of Skewed Mixing Layers, Technical Report TF-67, Department of Mechanical Engineering, Stanford University, Stanford, California, 1996.

Lu, G. & Lele, S.K. On the density ratio effect on the growth rate of a compressible mixing layer, *Physics of Fluids*, **6**, 1073-1075, 1994.

Publications to date with partial support from this grant:

Lele, S.K. Compressibility effects on turbulence, *Annual Review of Fluid Mechanics*, **26**, 211-254, 1994.

References

[1] D. A. Anderson, J. C. Tannehill, and R. H. Pletcher. *Computational Fluid Mechanics and Heat Transfer.* Hemisphere Publishing Co., New York, 1984.

[2] D. W. Bogdanoff. Compressibility effects in turbulent shear layers. *AIAA Journal*, 21: 926–927, 1983.

[3] R. J. Briggs. *Electron-Stream Interaction with Plasmas*, volume 29 of *Research Monograph.* MIT Press, Cambridge, 1964.

[4] P. E. Dimotakis. Turbulent free shear layer mixing and combustion. *GALCIT Report*, FM91-2, 1991.

[5] T. F. Fric. Skewed shear layer mixing within a duct. *AIAA paper*, Paper No. 95-0869, 1995.

[6] C. E. Grosch and T. L. Jackson. Inviscid spatial stability of a three-dimensional compressible mixing layer. *Journal of Fluid Mechanics*, 231: 35–50, 1991.

[7] H. Gründel and H. E. Fiedler. The mixing layer between non-parallel streams. In *The Fourth European Turbulence Conference*, pages 27–29, 1992.

[8] J. E. Hackett and D. K. Cox. The three-dimensional mixing layer between two grazing perpendicular streams. *Journal of Fluid Mechanics*, 43: 77–96, 1970.

[9] M. G. Hall. The structure of concentrated vortex cores. *Progress in Aeronautical Sciences*, 7: 53–110, 1966.

[10] S. K. Lele. Compact finite difference schemes with spectral-like resolution. *Journal of Computational Physics*, 103: 16–42, 1992.

[11] D. Papamoschou and A. Roshko. The compressible turbulent shear layer: an experimental study. *Journal of Fluid Mechanics*, 197: 453–477, 1988.

[12] N. D. Sandham and W. C. Reynolds. A numerical investigation of the compressible mixing layer. Technical Report TF-45, Department of Mechanical Engineering, Stanford University, Stanford, California, 1989.

[13] K. W. Thompson. Time dependent boundary conditions for hyperbolic systems. *Journal of Computational Physics*, 68: 1–24, 1987.

[14] K. W. Thompson. Time dependent boundary conditions for hyperbolic systems. *Journal of Computational Physics*, 89: 439–461, 1990.

[15] A. A. Wray. Very low storage time-advancement schemes. Internal report, NASA-Ames Research Center, Moffett Field, California, 1986.

[16] A. A. Wray. Vectoral manual. Internal report, NASA-Ames Research Center, Moffett Field, California, 1988.

Appendix
Inviscid Instabilities of a Curved Compressible Mixing Layer

Sanjiva K. Lele and Calvin Lui
Dept. of Mechanical Engineering
Stanford University, Stanford, CA 94305-4035.

The primary objective of this work was to evaluate the impact of mean streamline curvature on the unstable modes of a compressible mixing layer. The aim was to obtain a quick assessment of the potential destabilization offered by adding a moderate amount of curvature to the mean flow of a compressible mixing layer. A schematic of the flow considered is shown in figure A1. The mean flow profiles were taken as simple curve fits to known behavior on the two sides of the mixing region. Systematic exploration of the effect of streamline curvature and compressibility were carried out. Two main conclusions were reached. Firstly, the addition of destabilizing curvature increases the growth rate of the basic shear layer instability (Kelvin-Helmholtz mode). This increase is modest under incompressible conditions ($5-7\%$ curvature increases the growth rate by $30-50\%$). However, the destabilization is only weakly affected by compressibility and since the basic shear layer instability is strongly stabilized by compressibility (Papamoschou and Roshko, 1988) the destabilization can have a large impact on the growth under compressible conditions. For the case shown in figure-A2 for mixing between streams of velocity ratio $U_2/U_1 = 0.5$, $\rho_2/\rho_1 = 0.5$ and $M_1 = 4.0, M_2 = 0.38$ the addition of 7% curvature increases the growth rate of the basic K-H instability to about *three times* the growth rate without curvature. Also evident in the figure is the large impact of even mild curvature (1%) on the growth rate.

The second conclusion concerns the new modes of instability which destabilizing curvature adds to the mixing layer, viz. the Taylor Görtler vortices which appear as modes with zero temporal frequency but finite spanwise wavenumber. Figure-A3 shows that the growth rate of the T-G modes is largely insensitive to compressibility, and further their growth rate at modest levels of curvature is comparable or superior to the basic K-H mode (which as noted earlier is also destabilized by curvature).

These two facts taken togather point to a significant mixing enhancement potential offered by curving the mean streamlines in mixing under compressible conditions. This result should be of significant interest to propulsion applications which seek such mixing enhancement. Supersonic jet noise reduction and rapid mixing of engine/rocket plumes are other areas where the current results would be of interest.

Figure A1: Schematic of Curved Mixing Layer

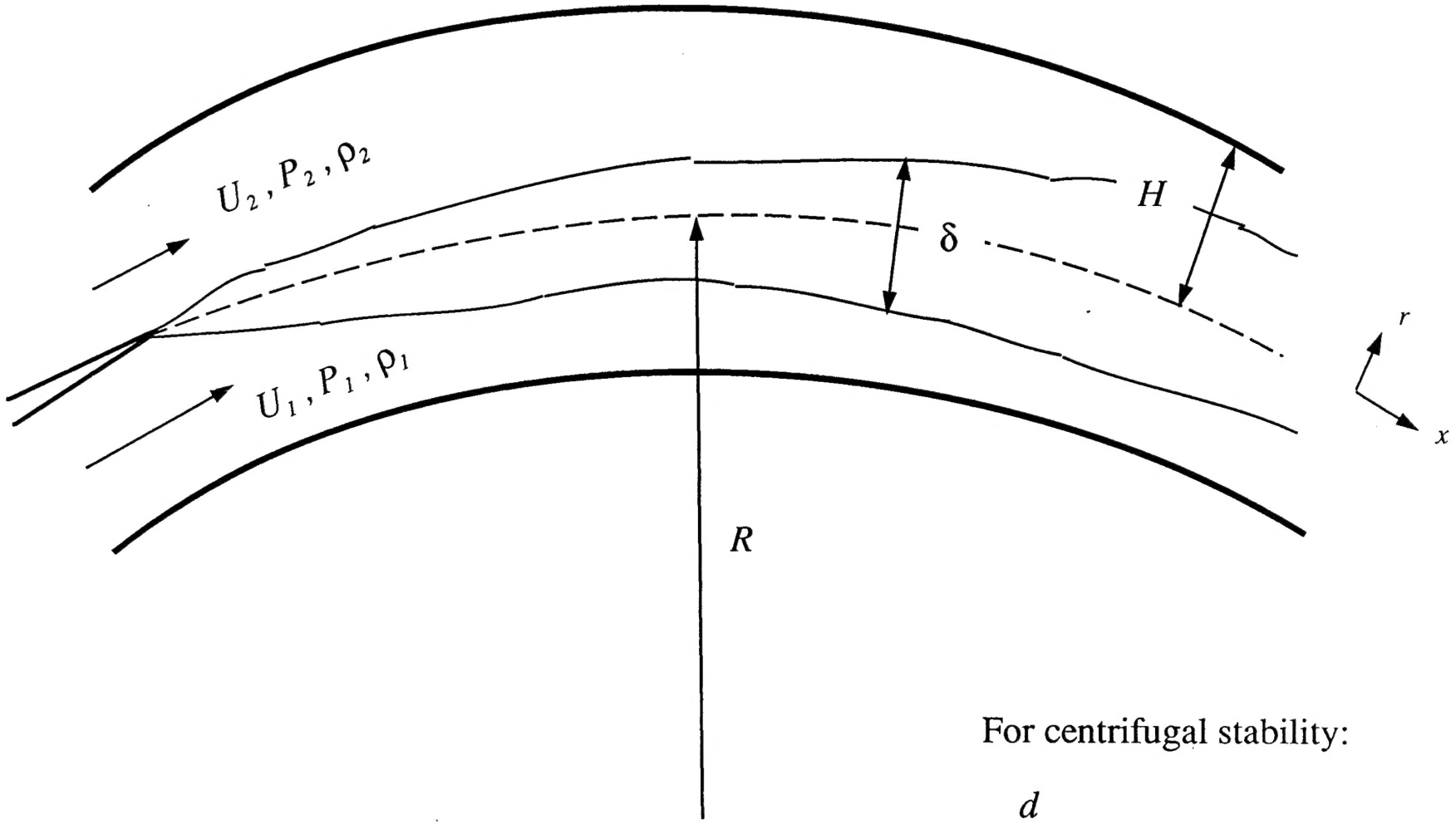

For centrifugal stability:

$$\frac{d}{dr}(\rho\, u^2\, r^2) > 0$$

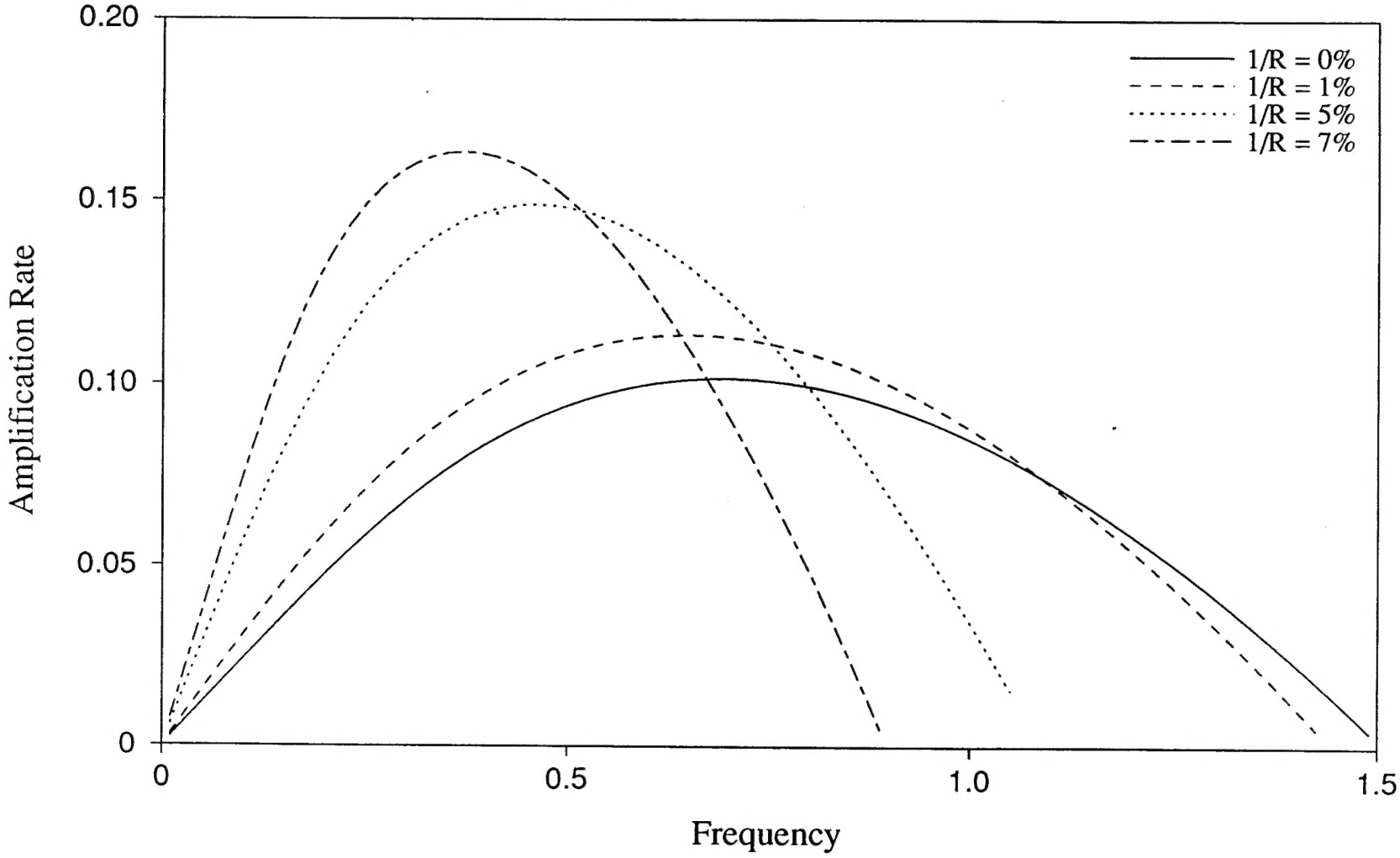

Figure A2a: Curvature Effects on Two–Dimensional Kelvin–Helmholtz Mode at Mild Compressibility
(Γ_2=0.5, ρ_2=0.5, M_1=2.0)

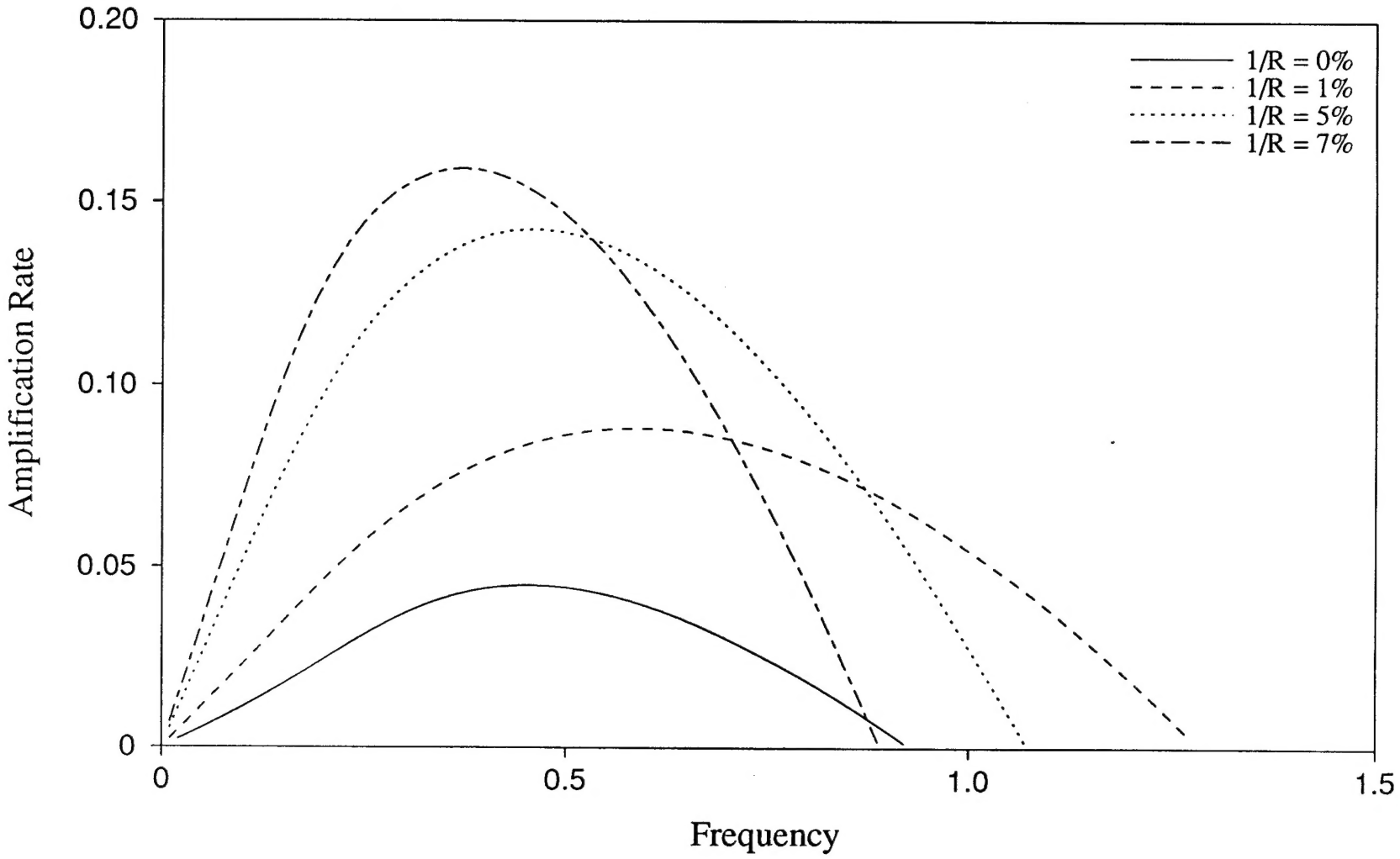

Figure A2b: Curvature Effects on Two–Dimensional Kelvin–Helmholtz Mode at High Compressibility (Γ_2=0.5, ρ_2=0.5, M_1=4.0)

Figure 3a: Incompressible Oblique Modes (M1=0.01)

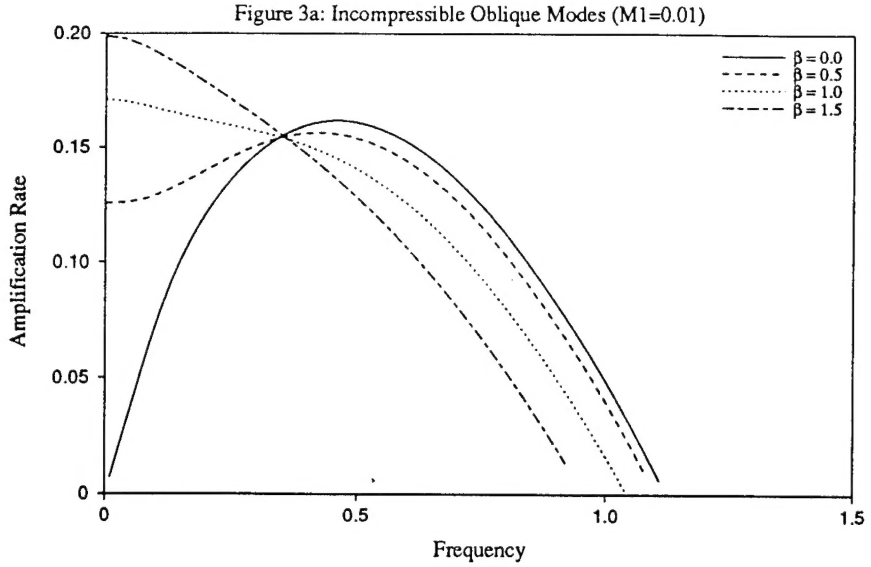

Figure 3b: Mildly Compressible Oblique Modes (M1=2.0)

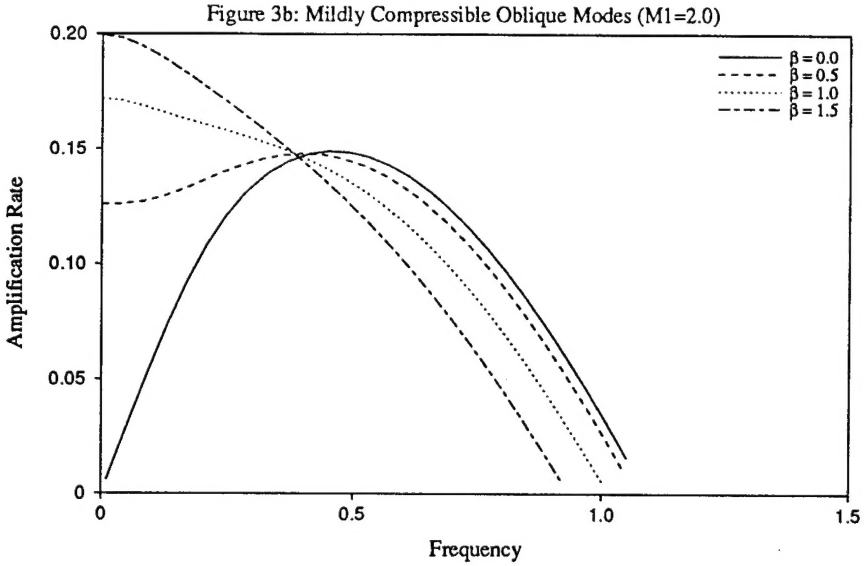

Figure 3c: Compressible Oblique Modes (M1=4.0)

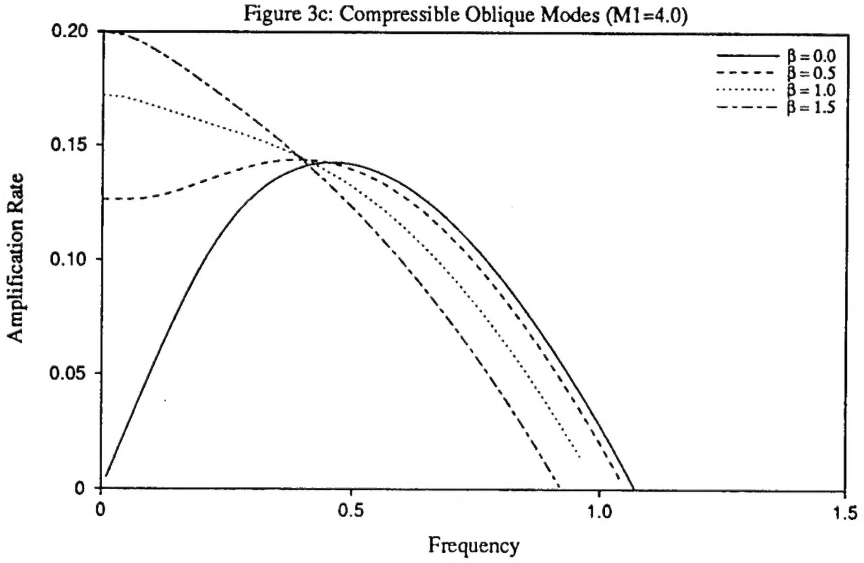

Figure A3: Compressibility Effects on Oblique Modes (Γ_2=0.5, ρ_2=0.5, 1/R=5%)

β: spanwise wave number